arXiv:2412.11247v1 [physics.optics] 15 Dec 2024

Interface and spectrum multiplexing Ptychographic reflection microscopy

Yun Gao[a], Qijun You[a], Wei Cao[a,*] and Peixiang Lu[a,d]

[a] *School of Physics and Wuhan National Laboratory for Optoelectronics, Huazhong University of Science and Technology, Wuhan, 430074, China*
[d] *Optics Valley Laboratory, Wuhan, 430074, China*

ARTICLE INFO

Keywords:
lensless imaging
coherent diffractive imaging
optical metrology

ABSTRACT

Reflective ptychography is a promising lensless imaging technique with a wide field of view, offering significant potential for applications in semiconductor manufacturing and detection. However, many semiconductor materials are coated with different layers during processing, which leads to the reflected diffraction light being a coherent superposition of multiple light beams. Traditional phase recovery methods often overlook the multi-layered nature of these materials, resulting in artificial errors and, in some cases, failures in image reconstruction. This limitation has hindered the broader application and adoption of reflection ptychography. Here, we propose and experimentally demonstrate an innovative interface and spectrum multiplexing ptychographic reflection microscopy. By employing multi-wavelength light as the illumination source, our approach enables the accurate extraction of the wavelength-dependent surface structure imaging and topography mapping of materials in a single experiment. This advancement offers a reliable technique for element-specific detection of semiconductor materials, utilizing tabletop extreme ultraviolet light sources in the future.

1. Introduction

As one of the lensless imaging techniques, coherent diffraction imaging(CDI) simultaneously recovers both the intensity and phase information of samples[1], making it highly valuable in biomedicine, materials science, and electronic devices research[2; 3; 4; 5; 6]. The technique which offers higher spatial resolution, a certain depth of nondestructive penetration, and chemical sensitivity[7; 8; 9; 10], opens more possibilities for the advancement of nanomaterials and nanotechnology. Through the overlap between different probing points, ptychography greatly improves the robustness on the basis of the original coherent diffractive imaging. The increasing redundancy allows fewer prior conditions of the illumination, decoupling of different incoherence illumination, object, and noise modes[11; 12; 13].

Reflection ptychography offers superior performance compared with transmission ptychography, especially for relatively thick, opaque samples and high-contrast phase imaging applications. It provides valuable insights into surface morphology, elemental composition specificity, and buried interface structures[14; 15; 16; 17; 8]. Particularly relevant in the semiconductor industry and nanofabrication technologies, utilizing ptychography enables non-destruc tive and penetrating examination of silicon-based chips to a certain depth, allowing for high-resolution imaging while addressing the optical component processing challenges in the extreme ultraviolet(EUV) spectrum[18; 19]. Therefore, the continued development of reflection ptychography is essential for advancing these technologies.

However, our investigation has identified a significant challenge in imaging various practical samples, such as silicon-based chips and biomaterials, using ptychographic reflection microscopy. The intrinsic properties of these materials, along with their fabrication processes, often result in top surface reflectivities that are less than 100%. Consequently, the portion of the transmitted probe reflects from various interfaces in a mutually coherent manner, complicating the diffraction information obtained with multiple probes. While some approaches aim to utilize multiple spatially or spectrally separated illuminations, each of which still ensures a certain degree of coherence, can reconstruct different object functions and illumination functions as different modes. These methods typically rely on the mutual incoherence between different illumination modes[11; 12; 13]. In contrast, the exited waves reflected from different interfaces cannot be considered separate incoherent modes, as seen in temporally multiplexed multibeam ptychographic imaging [20]. Furthermore, the intermingling of information from various interfaces complicates the reconstruction process. Consequently, current multi-mode ptychography algorithms, which could reconstruct multiple incoherent modes simultaneously, fail to effectively decouple multiplexed interface information within this reflection geometry. These complexities in reflection ptychography frequently fail reconstruction, posing a significant challenge and hindering the widespread adoption of reflection ptychography. Thus, more rigorous data processing and reconstruction processes for reflection ptychography are necessary.

In order to solve the above problems, in this article, we propose an imaging scheme called interface and spectrum multiplexing ptychographic reflection microscopy(PISM), which firstly considers the interference of multiple reflected waves brought by the inherent issues or lamellar structures of samples and information coupling caused by it. This approach not only enables accurate surface structure imaging but also extends functionality to spectral response analysis.

---

*Corresponding author
`weicao@hust.edu.cn` (W. Cao)
ORCID(s):

The different wavelengths of light interacting with the etched film and nanostructure lead to interference cancellation or interference phase, resulting in distinct imaging results of the sample. Therefore, we incorporate spectrum multiplexing for the chip inspection. PISM can also be applied to single-shot ptychographic imaging[21; 22]with a wide field of view, without needing to separately account for aperture distances to ensure incoherence between beams. We demonstrated the effectiveness of this method using measured data from two respective samples, a negative 1951 resolution test chart, and an abandoned chip.

The successful acquisition of spectral and spatial multiplexing information in the system has been achieved, proving that our work ensures the correction of samples' reconstruction and solves the artifact problem that often occurs in reflection ptychography imaging. The advancement overcomes a key barrier to the widespread application of reflection ptychography imaging and provides technical support for surface morphology diagnosis, nondestructive detection, and material identification. When combined with the characteristics of extreme ultraviolet and X-ray technologies, technology will show more significant potential for enabling full 3D dynamic ptychographic imaging in nanotechnology.

2. Results

2.1. Interfaces and spectrum multiplexing Ptychographic reflection microscopy methodology

Consider the two beams $\Psi_1(r)$ and $\Psi_2(r)$ carrying information from different interfaces of the sample are mutually coherent and scatter to the far field accepted by the detector. At this time, the diffraction pattern is recorded as:

$$\begin{aligned} I(k) &= |\mathcal{F}[\Psi(r)]|^2 \\ &= \left|\mathcal{F}[\Psi_1(r)+\Psi_2(r)]\right|^2 \\ &= \left|\widetilde{\Psi}_1(k)\right|^2 + \left|\widetilde{\Psi}_2(k)\right|^2 + \widetilde{\Psi}_1(k)\widetilde{\Psi}_2(k)^* + \widetilde{\Psi}_1(k)^*\widetilde{\Psi}_2(k) \end{aligned} \tag{1}$$

where$\mathcal{F}$ is the 2D Fourier transform operator and $\widetilde{\Psi}$ is the form of Ψ after Fourier transform. Mutual interference between the adjacent beams introduces two coherent terms. The existing multi-mode decoupling method, which considers the diffraction intensity to be simply the sum of incoherent modes, is not suitable anymore. Therefore, the influence of the interference should be eliminated first.

For samples with a thickness of the substrate, beams reflected from different interfaces will have a certain spatial translation with each other, just shown as [Fig. 1.b]). Applying this space interval, we eliminate the additional two terms in equation 1 by auto-correlation filtering. The whole data processing is shown in [Fig. 1.c-f]. Operating the Fourier transform to the diffraction intensity, the cross-correlation terms (framed in black in [Fig. 1.d]), originating from the interference terms are separated from the auto-correlation terms. Based on this, we can remove the isolated cross-correlation terms and then do the inverse Fourier transform to the left data, resulting in diffraction intensity free from the interference terms. In this way, the processed diffraction pattern can be regarded as an incoherent superposition of multiple beams reflected from various interfaces, then existing multi-mode ptychography algorithms can be applied.

The propagation process of light in the sample is shown in [Fig. 1.b]. Note in the reflected wave Ψ_2, the probe passes the sample twice complicating the reconstruction of probe's and sample's functions. We introduce the reflection ptychographic interface and spectrum multiplexing iteration method (PISM), which effectively decouples the information from different interfaces combining with the off-axis light propagation and principle of multi-slice approach[23]. In [Fig. 1.b], Ψ_1 is the beam that is reflected directly from the top and it can be expressed as: $P \cdot O_r$, where O_r is uppermost reflection function, P is the incident light. A portion of the light that does not reflect passes through the top surface of the sample, reflects back from the substrate and passes through the sample's top surface for another time. This is the second beam Ψ_2 and its expression can be written as: $\Psi_2 = H \langle P \cdot O_{t1} \rangle \cdot O_{t2}$, where H represents the tilt angular spectrum propagation in the substrate and O_{t1} the first transmission function,$O_{t2}$the second transmission function. Finally, these two beams interfere with each other and scatter onto the detector's receiving surface. Now, we rewrite the diffraction pattern as

$$\begin{aligned} I(k) &= |\mathcal{F}[\Psi(r)]|^2 \\ &= \left|\mathcal{F}[\Psi_1(r) + \mathcal{F}[\Psi_2(r)]\right|^2 \\ &= \left|\mathcal{F}(P \cdot O_r) + \mathcal{F}(H \langle P \cdot O_{t1} \rangle \cdot O_{t2})\right|^2 \\ &= \left|\mathcal{F}(P \cdot O_r)\right|^2 + \left|\mathcal{F}(H \langle P \cdot O_{t1} \rangle \cdot O_{t2})\right|^2 \end{aligned} \tag{2}$$

In the multi-slice approach, the transmitted probe propagated for a distance can be seen as a new probe in the form of $H \langle P \cdot O_{t1} \rangle$ for the next transmission. In that case, in each iteration, P_r, P_{t2} are recovered directly from Ψ_1,Ψ_2 respectively. P_{t1}can be attained through the other nested update based on the principles of the multi-slice approach. At the end, O, P_r, P_{t1}, $P_{t2}$are recovered simultaneously after certain number of iterations. As for the multi-wavelength diffraction intensity I_m is the integral over different wavelengths:

$$I(k)_m = \sum_{i=1}^{m} \left|\mathcal{F}(P^m O_r^m)\right|^2 + \left|\mathcal{F}(H \left\langle P \cdot O_{t1}^m \right\rangle \cdot O_{t2}^m)\right|^2 \tag{3}$$

2.2. Interfaces and spectrum multiplexing Ptychographic reflection microscopy setup

The schematic of our interfaces multiplexing ptychographic reflection microscopy is shown in [Fig. 1.a]. The collimated incident light passes through a 200nm precise pinhole and illuminates the sample which is mounted on a two-axis scanning stage. The small pinhole provided

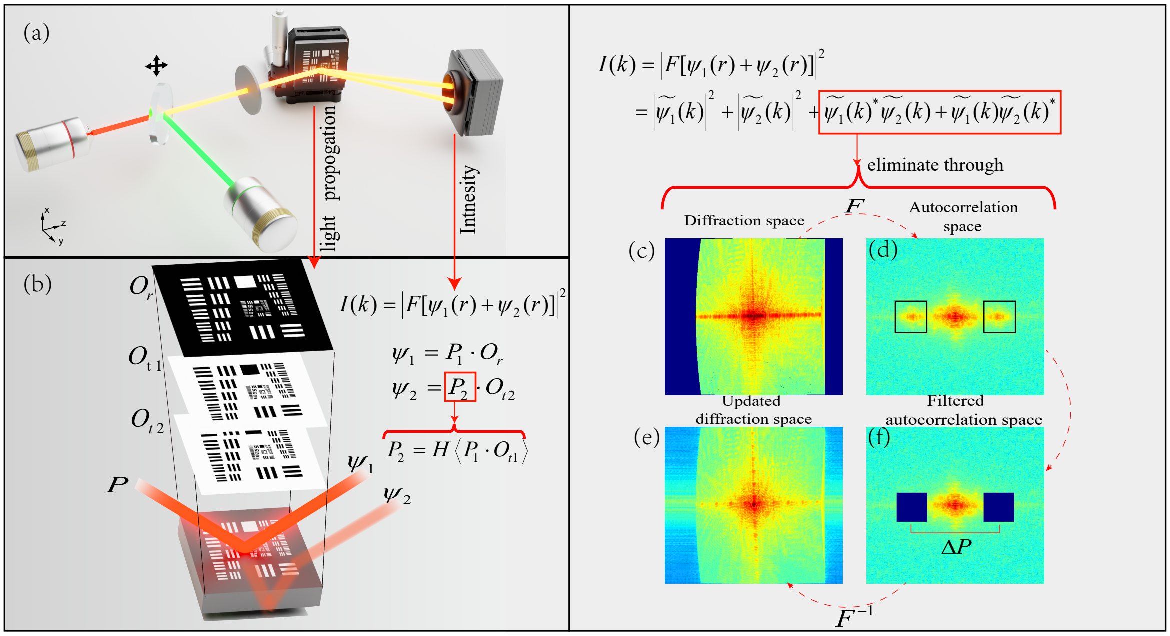
(a)
light propogation
Intnesity
(b)
O_r
O_{t1}
O_{t2}
P
ψ_1
ψ_2
$I(k) = |F[\psi_1(r)+\psi_2(r)]|^2$
$\psi_1 = P_1 \cdot O_r$
$\psi_2 = \boxed{P_2} \cdot O_{t2}$
$P_2 = H\langle P_1 \cdot O_{t1} \rangle$
$I(k) = |F[\psi_1(r)+\psi_2(r)]|^2$
$= |\widetilde{\psi_1}(k)|^2 + |\widetilde{\psi_2}(k)|^2 + \boxed{\widetilde{\psi_1}(k)^* \widetilde{\psi_2}(k) + \widetilde{\psi_1}(k)\widetilde{\psi_2}(k)^*}$
eliminate through
Diffraction space
F
Autocorrelation space
(c)
(d)
Updated diffraction space
Filtered autocorrelation space
(e)
(f)
ΔP
F^{-1}

Figure 1: Geography and methodology illustration of the reflective ptychography microscopy. (a) Geography of the reflective ptychography microscopy. (b) Light propogation in the sample. After the tilt correction[24], diffractive intensity is the squares of the Fourier transform of the sum of reflected waves Ψ_1 and Ψ_2. Each of the reflected waves is expressed based on the probe's function P, the sample's reflection function O_r, and transmission functions O_{t1}, O_{t2}. F is the 2D Fourier transform operator and $\widetilde{\Psi}$ is the form of Ψ after Fourier transform. H <> is the tilt angular spectrum propagator. (c)-(f) A flow chart of the autocorrelation filtering process: (b) The diffraction data after the tilt correction. (c) Data after a Fourier transform from the data in (b). (d) Data after removing the cross-correlation terms in (b). (e) Data after an inverse Fourier transforming the data in (d).

simple geometrical constraints as real space's support. Under normal circumstances, isolating a sample is indeed more challenging in a reflection-mode keyhole ptychography configuration than in a transmission-mode configuration due to the need to avoid light path occlusion. Scattered light from objects, which is the coherent superposition of multiple beams reflecting from different interfaces, was measured by a CCD detector placed 0.08 m away from the sample. To demonstrate the developed approach mentioned above, firstly, we performed experiments with 633nm monochromatic light(continuous-wave red laser) on a negative USAF1951 resolution test chart and an abandoned chip. We are particularly interested in the varying responses of the sample to different wavelengths, as influenced by the nanostructures of the materials, which is a common phenomenon in chip inspection and biomaterials imaging [25; 26]. To investigate this, we combine 532 nm monochromatic light with another 532 nm monochromatic light and illuminate the sample simultaneously, as shown in [Fig. 2.a]. The two beams, red and green, are combined using a beam splitter and then directed onto the sample through a precise pinhole. In all experiments, the angle between the incident light and the sample is 45 degrees. The recorded diffraction patterns were captured by a detector with 2048×2048 pixels and spliced from three exposure times to enlarge the dynamic range and increase the patterns' signal-to-noise ratio. The scanning form is an S-type detour and at each moving step, the fixed step size is superimposed with a random offset of about 10 percent of the aperture size to improve the recovery effect. In the monochromatic interfaces multiplexing reflection ptychography experiments, the overlap rate of 70-80 percent was chosen. Accordingly, to meet the redundancy requirement for the recovery of multiple modes, an overlap rate of 85 percent was selected for the additional spectrum multiplexing experiments.

2.3. Negative 1951 resolution test chart

We collected diffraction data from a negative 1951 resolution test chart using a reflection-based coherent diffraction imaging geometry with a 633nm monochromatic light. The reconstructed amplitudes of the imaged chart with the usual ptychography method—Douglas-Rachford algorithm(sDR)[27] and PISM algorithm are respectively shown in the [Fig.2.a,c]. As illustrated in [Fig.2.a], after correcting the tilt diffraction data, the recovered object image by sDR exhibits strong interference between two beams originating from two different interfaces, and the corresponding two probes are simultaneously reconstructed, as shown in [Fig.2.b]. These erroneous features are highlighted by red lines in [Fig. 2.a,b]. It is evident that the recovered object consists of a mixture of the transmission function (right part of [Fig.2.a]) and the reflection function (left part of [Fig.2.a]). While after the improved reconstruction procedures, the error is corrected and all the information P, O_r, O_{t1}, O_{t2} are differentiated and recovered as shown in the [Fig. 2.c-f]. Since the sample is a negative test target, meaning that a higher proportion of light intensity is reflected back while less is transmitted into the substrate, the transmitted light intensity gradually decreases

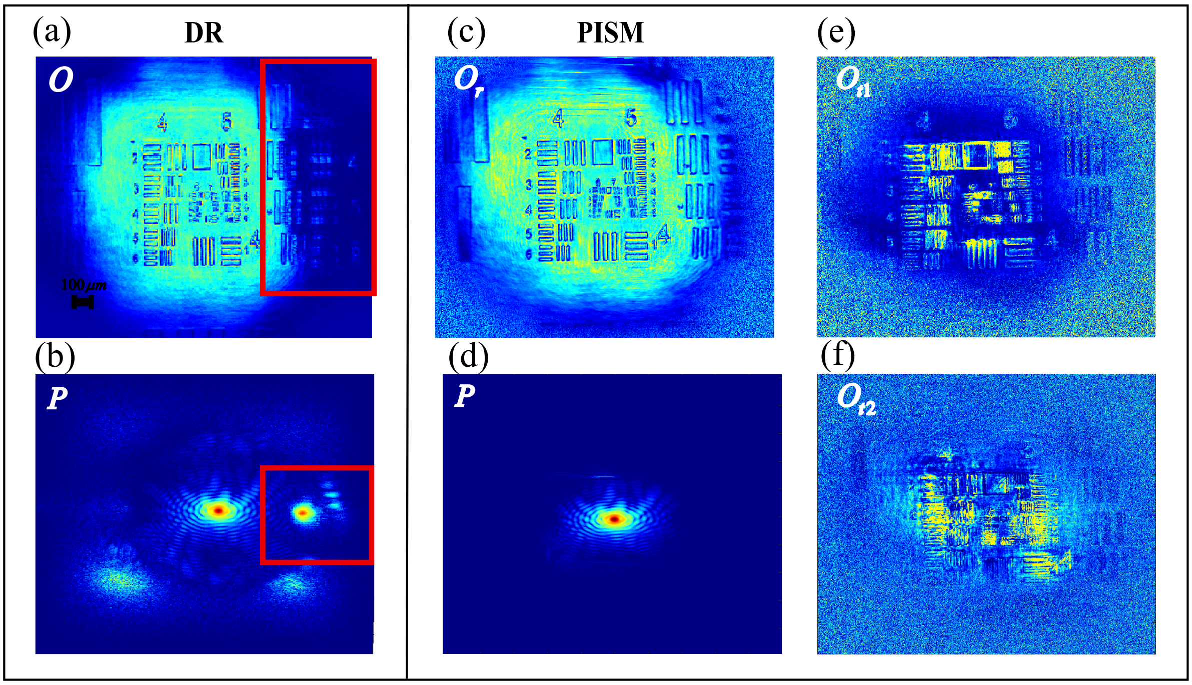

Figure 2: Reconstructions of negative reflective 1951 resolution test chart for the 633nm monochromatic source. (a)-(b) Reconstructions by sDR. (c)-(f) Reconstructions by PISM: (c)the recovered reflection amplitude information of the sample from$|\Psi_1|$, (d) the recovered probe, (e)-(f)the recovered transmission amplitude information of the sample from $|\Psi_2|$

during propagation. Consequently, the signal-to-noise ratio of the scattered signal also diminishes. As a result, the two reconstructed transmission images exhibit poorer performance compared to the reflection image, particularly at the edges of the recovered images. This degradation occurs because, after the probe with an Airy spot shape has propagated over a certain distance, the intensity at the edges is significantly attenuated. However, the reconstructed transmission result at the first interface, P_{t1} can still guarantee a certain resolution. It is worth mentioning that we used the same overlap rate as in conventional ptychographic imaging experiments, ensuring the same level of robustness. However, our method recovers richer and more accurate information about the sample.

Different wavelengths of light interacting with etched films and nanostructures lead to different imaging results. To observe the structures that cannot be observed in some wavelengths, the technique extends functionality to multi-wavelength multiplexing with the dual-wavelength experiment. The data processing in [Fig.1.c-f] and the new image reconstruction procedure PISM are operated in the dual-wavelength experiment, in which the 532nm and 633nm narrow continuous wavelength lasers are combined to illuminate the chart at the same time. Since the exposure time of the image sensor is longer than the period of each of the two pulses, the solution to different wavelengths is consistent with the Ψ_1, Ψ_2 which can be considered two incoherent modes, so the diffraction intensity can be regarded as the incoherent superposition of four modes in total. The recovered reflection amplitude and phase images for dual laser sources are given in [Fig. 3]. It can be seen from three groups of test chart reconstructions that the experimental imaging effect of multi-wavelength is nearly the same as that of monochrome ones. The resolution of the sample is determined by both numerical aperture(NA) and wavelength. Due to the shorter wavelength, the resolution of red light is lower than that of green light, which aligns with the recovered results shown in [Fig. 3.], that the 6,7 groups of test targets in [Fig. 3.b] are slightly fuzzier than them in [Fig. 3.a]. Additionally, the recovered images of the test target strokes for red and green light exhibited slightly different contrasts between the coating and the substrate, as the intensity of light reflected from the substrate differs at different wavelengths. This issue has been observed in many multi-wavelength reflection ptychography imaging experiments with varying intensity ratios, indicating that the observed differences are objective.

2.4. Abandoned chip

The same reflection ptychography imaging geometry is applied to an abandoned chip sample with some etched patterns on the surface. Both in the monochromatic experiment and the dual-light experiment, after operating the

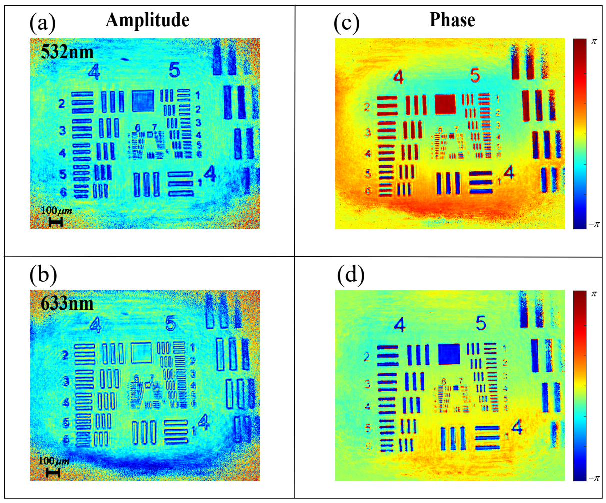

Figure 3: Reconstructions of reflective 1951 resolution test chart for the 532nm and 633nm sources. (a) The recovered reflection amplitude information for 532nm light. (b) The recovered reflection amplitude information for 633nm light. (c) The recovered reflection phase information for 532nm light. (d) The recovered reflection phase information for 633nm light.

Fast Fourier transform to the scattered intensity, in the autocorrelation space, there are two additional cross-items transformed from the interference items, which have been marked in black boxes shown in [Fig. 4.a], which means the similar interference probably between the surface reflection beam and the substrate reflection beam exists. Therefore, data was processed identically to the last experiment and then, we applied the developed approach PISM to reconstruct the amplitude and phase information of the chip and probe. The recovered probe's amplitude and chip surface structure with a 633nm light source are shown in [Fig. 4.b-d].

The reconstructed amplitudes of the probes and objects in the dual-wavelength experiment are shown in [Fig. 5]. Notably, the reconstruction of the raster-like structure etched on the right side of the chip under red light illumination at an incident angle of 45° is less pronounced compared to the reconstruction under green light illumination. These results clearly demonstrate that the chip exhibits different reflected intensity distributions depending on the wavelength used. Furthermore, in this experiment, the object function reconstructed in the red light mode shows a relatively lower resolution compared to the result obtained in the aforementioned red light monochromatic experiment. This can be attributed to the fact that more modes share the signal-to-noise ratio in the dual-wavelength experiment. Additionally, under reflection illumination, the chip's spectral response to green light is significantly stronger than its response to red light, which is evident in the diffraction data, resulting in a higher signal-to-noise ratio for the green light mode compared to the red light mode.

3. Discussion

We compare our reconstructed images to the metallographic microscope and SEM(ZEISS EVO 10) at the same area of the chip. All results are basically agree except for some raster-like structures on the right of the field. These structures are discernable in reconstructed amplitude and phase of ptychography imaging but cannot be distinguished very well in SEM due to the concession to the field of view.

Previous work using the autocorrelation filtering process has shown that the process of diffraction data has no noticeable effect and information loss on the reconstructed resolution of the object function[28]. To numerically characterize the resolution of the microscope, we chose a profile in x-axial in [Fig. 4.a] and measured the 10%-90% width of it. Specific analysis is added to the supplement materials.

Reflection ptychography is also an effective technique to attain quantitative surface profiling with high sensitivity to phase. To determine the propagation-axial height resolution, we calculate the height information from the phase reconstructions using prior information such as wavelength, incidence angle, and composition. The wavelength-dependent topography mapping of the chip made from the reconstructed phase of 532nm mode in the dual-wavelength experiment is shown in [Fig. 6.a]. Due to the lack of absolute phase reference, relative height information can be obtained. The specific heights of the surface structures are still accessible from it. We extract the height information of the feature area that has a stepped height transition (marked with the red box in [Fig. 6.a] using an atomic force microscope(AFM)(Nanosurf Flex-Mount), and compared it with the reconstructed height distribution using reflection ptychography. The histograms for the height values within this feature area are shown in [Fig. 6.b] and [Fig. 6.c]. Both histograms have a good agreement, indicating that the height difference of this stepped structure is approximately 400nm.

Based on all the discussion above, for reflection ptychography, applying a normal ptychography algorithm to get the recovered images of the object and probe can cause the wrong results or a failed reconstruction. We propose the new interface and spectrum multiplexing ptychographic reflection microscopy which for the first time considers the complex interference from different interfaces and responses to the spectrum. We demonstrate the method can realize reliable and accurate reflection information and topography mapping of samples through two samples' imaging experiments. It is believed it will promote reflection lensless phase imaging widely and we expect that the method will be combined with the extreme ultraviolet light source to play an important role in high-resolution space-time exploration.

4. Material and Methods

4.1. Auto-correlation filtering

In autocorrelation space, that is, after the Fourier transform of the diffraction intensity, the information is written

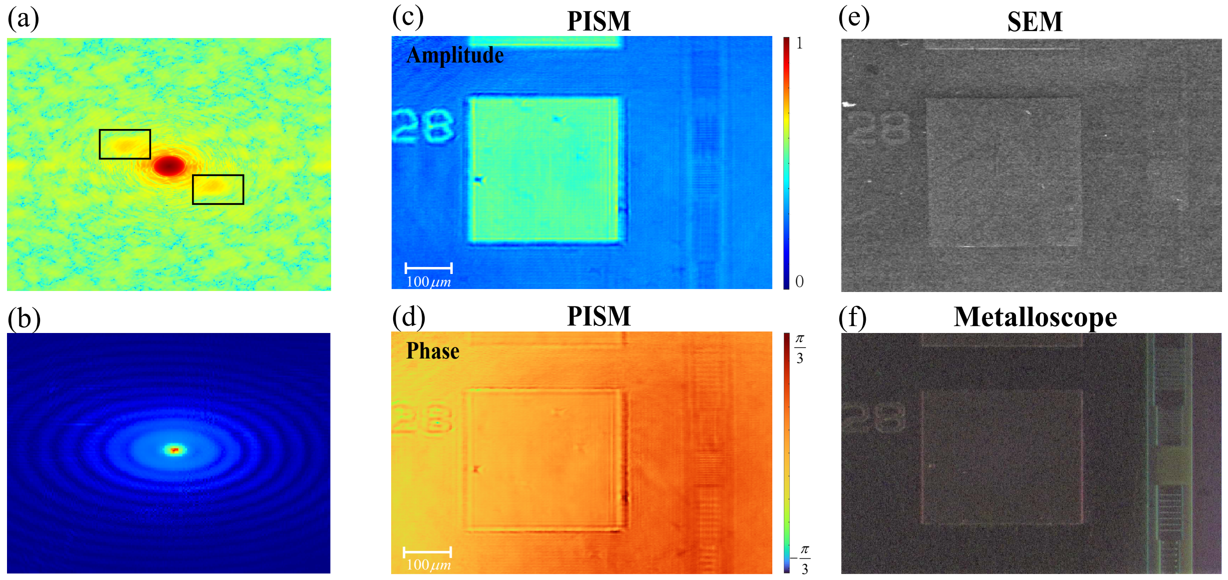

Figure 4: Data and reconstructions of the abandoned chip for monochromatic source with PISM algorithm. (a) Data after the Fast Fourier transform of the intensity. (b) The recovered probe by the PISM algorithm. (c) The recovered amplitude of the object reflection function by the PISM algorithm. (d) The recovered phase of object reflection function by PISM algorithm. (e)Scanning electron microscopy (SEM) image of the same area on the chip. (f)Metallographic of the same area on the chip.

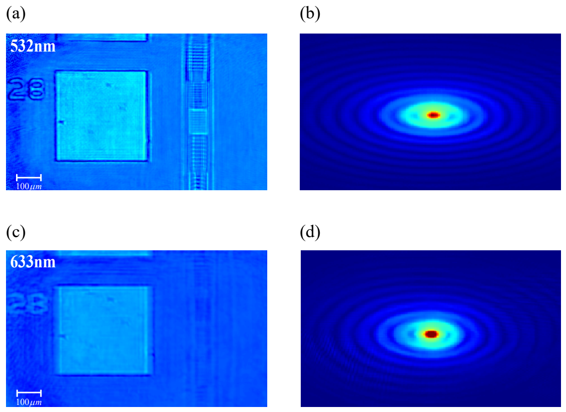

Figure 5: Reconstructions of abandoned chip for multi-wavelength source by PISM algorithm. (a)(b) The recovered amplitude of object reflection and probe function with a 532nm light source. (b)(d) The recovered amplitude of object reflection and probe function with a 633nm light source.

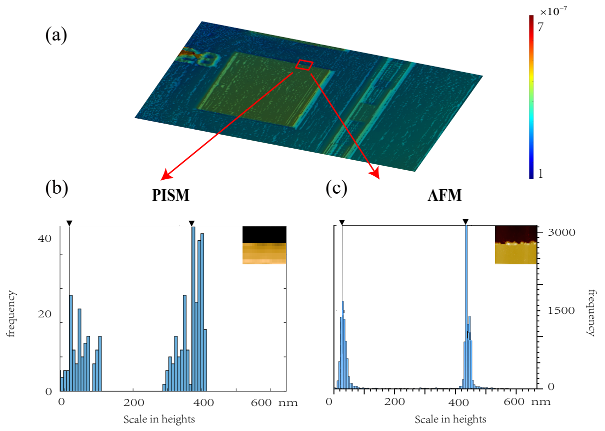

Figure 6: Height analysis based on interfaces and spectrum multiplexing ptychographic reflection microscopy and AFM. (a) Topography mapping by the interfaces and spectrum multiplexing ptychographic reflection microscopy. (b)Histogram of the interfaces and spectrum multiplexing ptychographic reflection microscopy. (The small picture in the upper right corner is the reconstruction in [Fig. 6) (c)Histogram of AFM (small picture in the upper right corner is the AFM image)

as:

$$\mathcal{F}[I(k)] = \Psi_1(r) \star \Psi_1(r) + \Psi_2(r) \star \Psi_2(r) + \Psi_1(r) \star \Psi_2(r)^* + \Psi_1(r)^* \star \Psi_2(r) \tag{4}$$

where $\star$ is the 2D auto-correlation operator and * indicates the complex conjugatation.

Express $\Psi_1(r)$ as $\Psi_1(r) = P_1(r - R_j)O_1(r)$ and $\Psi_2(r)$ as $\Psi_2(r) = P_2(r - R_j - \Delta r)O_2(r)$, where $\Psi_1(r)$, $\Psi_2(r)$ are two exited waves. $O_1(r)$, $O_2(r)$ are object functions in scan positionR_j. P_1, P_2 are probe functions of $\Psi_1(r)$ and $\Psi_2(r)$. Δr is the distance between two exit waves.

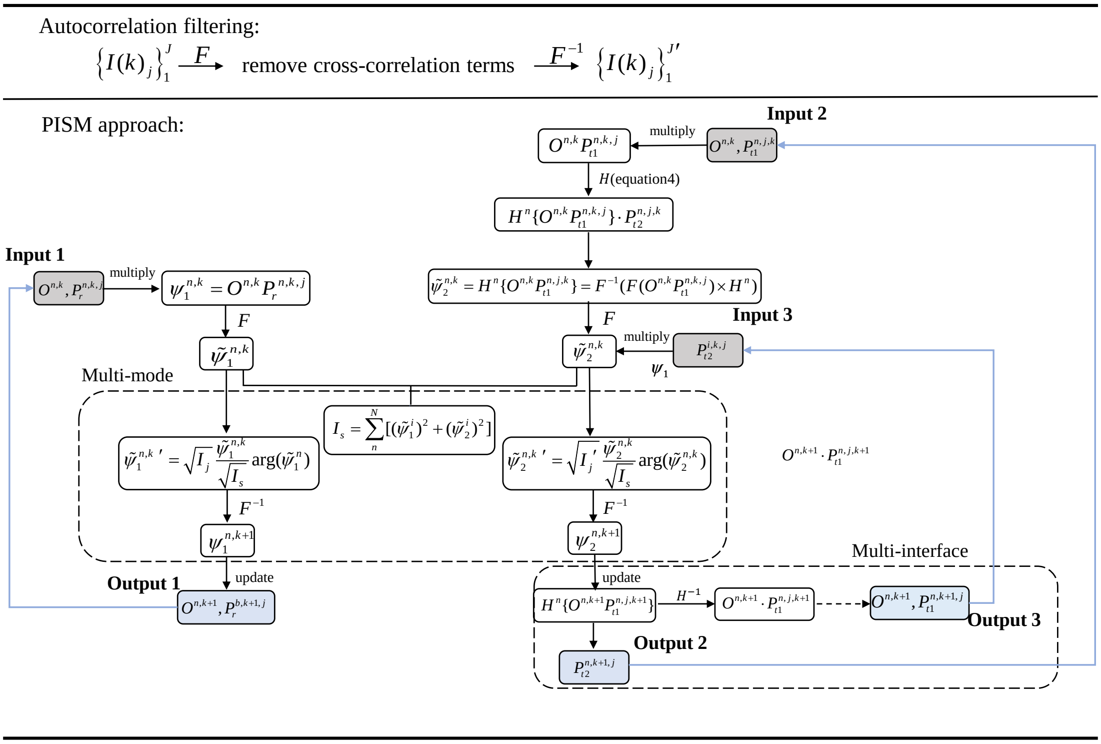
Autocorrelation filtering:
$\{I(k)_j\}_1^J \xrightarrow{F}$ remove cross-correlation terms $\xrightarrow{F^{-1}} \{I(k)_j\}_1^{J'}$
PISM approach:
Input 1
$O^{n,k}, P_r^{n,k,j}$
multiply
$\psi_1^{n,k} = O^{n,k} P_r^{n,k,j}$
F
$\tilde{\psi}_1^{n,k}$
Input 2
$O^{n,k}, P_{t1}^{n,j,k}$
multiply
$O^{n,k} P_{t1}^{n,k,j}$
H(equation4)
$H^n\{O^{n,k} P_{t1}^{n,k,j}\} \cdot P_{t2}^{n,j,k}$
$\tilde{\psi}_2^{n,k} = H^n\{O^{n,k} P_{t1}^{n,j,k}\} = F^{-1}(F(O^{n,k} P_{t1}^{n,k,j}) \times H^n)$
F
Input 3
multiply
$P_{t2}^{i,k,j}$
ψ_1
$\tilde{\psi}_2^{n,k}$
Multi-mode
$I_s = \sum_n^N [(\tilde{\psi}_1^i)^2 + (\tilde{\psi}_2^i)^2]$
$\tilde{\psi}_1^{n,k\,\prime} = \sqrt{I_j} \frac{\tilde{\psi}_1^{n,k}}{\sqrt{I_s}} \arg(\tilde{\psi}_1^n)$
$\tilde{\psi}_2^{n,k\,\prime} = \sqrt{I_j'} \frac{\tilde{\psi}_2^{n,k}}{\sqrt{I_s}} \arg(\tilde{\psi}_2^{n,k})$
$O^{n,k+1} \cdot P_{t1}^{n,j,k+1}$
F^{-1}
$\psi_1^{n,k+1}$
F^{-1}
$\psi_2^{n,k+1}$
Multi-interface
update
Output 1
$O^{n,k+1}, P_r^{b,k+1,j}$
update
$H^n\{O^{n,k+1} P_{t1}^{n,j,k+1}\}$
H^{-1}
$O^{n,k+1} \cdot P_{t1}^{n,j,k+1}$
$O^{n,k+1}, P_{t1}^{n,k+1,j}$
Output 3
Output 2
$P_{t2}^{n,k+1,j}$

Figure 7: A flow chart of the algorithm used by the interfaces and spectrum multiplexing Ptychographic reflection microscopy.

Then, equation 5 can be further written as:

$$\begin{aligned}\mathcal{F}[I(k)] = {} & P_1(r-R_j)O_1(r) \star P_1(r-R_j)O_1(r) + \\ & P_1(r-R_j)O_1(r) \star P_2(r-R_j-\Delta r)O_2(r) + \\ & P_1(r-R_j)O_1(r) \star P_2(r-R_j-\Delta r)O_2(r)^* \otimes \delta(r+\delta r) + \\ & P_1(r-R_j)O_1(r) \star P_2(r-R_j-\Delta r)O_2(r) \otimes \delta(r-\delta r)\end{aligned} \tag{5}$$

where $\otimes$ is the 2D convolution operator. As shown in [Fig. 1.c], due to the spatial separation in the X-axis directionΔx between Ψ_1 and Ψ_2 in real space, there is a corresponding separation ΔP between the center of two cross-correlation terms and auto-correlation terms in auto-correlation space[28; 29; 30]. The mapping of Δx over the number of pixels can be expressed as $\Delta P = \Delta x D/\lambda Z$. By utilizing the numerical relationship, the spatial distribution of the exit waves can be determined. Removing the isolated area shown in the auto-correlation space in the figure(two blackened squares) and operating the inverse Fourier transform for another time, we can filter out the excess interference terms. [Fig. 1.c-f] the whole process of data processing of the autocorrelation filter after the tilt correction. Through autocorrelation filtering, corrected diffraction pattern can be transformed into the sum of incoherent terms, and then multi-mode ptychography algorithms like PIM, and mix-state can be used to recover the magnitude and phase information of probe and object as different modes simultaneously.

4.2. Off-axis light propagation

In the multi-slice approach, the propagated exit wave of the first transmission $H\langle P \cdot O_{t1}\rangle$ is computed as the incident wave for the next transmission. In terms of the off-axis light propagation between parallel layers of the sample with an arbitrary angle, a numerical method named Translated-angular spectrum method(Translated-ASM)[31] was used to accurately calculate diffraction fields in the disparate interfaces. The propagation of the exit wave function$P \cdot O_{t1}$ can be described by the Translated-angular spectrum function:

$$\Psi_0(x', y'; Z) = \mathcal{F}^{-1}(\mathcal{F}(E_i(x, y; 0)))exp(i\widetilde{k}_z R)[k_x, k_y] \tag{6}$$

In each iteration, P_r, P_{t2} ,shown in [Fig. 1.a]are recovered directly from Ψ_1,Ψ_2 respectively. Since P_{t1} is related to the probe of Ψ_2, P_{t1}can be attained through the other nested update based on the principles of the multi-slice approach. At the end, O, P_r, P_{t1}, $P_{t2}$are recovered simultaneously after certain number of iterations.

4.3. Iterative recovery process

As for the iterative recovery process, because the reflection-mode ptychography geometry uses the precise pinhole as support, the probe would be a non-standard circular diffraction, so we choose the Douglas-Rachford algorithm(sDR), which has better performance in practical applications, especially for relatively complex situations with limited prior information of the probe. All the phase iterative recovery procedure is detailed in[Fig. 7].

4.4. Materials

The abandoned chip sample is a silicon-based chip, which is a bad sheet produced during the chip production process, and the surface has some nanometer and micron layers and lithographic patterns.

Funding

NationalNatural Science Foundation of China(12274158).

National Key Research and Development Program of China(2023YFA1406800).

References

[1] Jianwei Miao, Pambos Charalambous, Janos Kirz, and David Extending the methodology of x-ray crystallography to allow imaging of micrometre-sized non-crystalline specimens. 400(6742):342–344, 1999.

[2] David Shapiro, Pierre Thibault, Tobias Beetz, Veit Elser, Malcolm Howells, Chris Jacobsen, Janos Kirz, Enju Lima, Huijie Miao, Aaron M. Neiman, and David Sayre. Biological imaging by soft x-ray diffraction microscopy. 102(43):15343–15346, 2005.

[3] Changyong Song, Raymond Bergstrom, Damien Ramunno-Johnson, Huaidong Jiang, David Paterson, Martin D De Jonge, Ian McNulty, Jooyoung Lee, Kang L Wang, and Jianwei Nanoscale imaging of buried structures with elemental specificity using resonant x-ray diffraction microscopy. 100(2):025504, 2008.

[4] Ashish Tripathi, Jyoti Mohanty, Sebastian H. Dietze, Oleg G. Shpyrko, Erik Shipton, Eric E. Fullerton, Sang Soo Kim, and Ian McNulty. Dichroic coherent diffractive imaging. 108(33):13393–13398, 2011.

[5] Ofer Kfir, Sergey Zayko, Christina Nolte, Murat Sivis, Marcel Möller, Birgit Hebler, Sri Sai Phani Kanth Arekapudi, Daniel Steil, Sascha Schäfer, and Manfred Nanoscale magnetic imaging using circularly polarized high-harmonic radiation. 3(12):eaao4641, 2017.

[6] Joanne Marrison, Lotta Räty, Poppy Marriott, and Peter O'Toole. Ptychography – a label free, high-contrast imaging technique for live cells using quantitative phase information. *Scientific Reports*, 3(1):2369, 2013.

[7] Dennis F. Gardner, Michael Tanksalvala, Elisabeth R. Shanblatt, Xiaoshi Zhang, Benjamin R. Galloway, Christina L. Porter, Robert Karl Jr, Charles Bevis, Daniel E. Adams, Henry C. Kapteyn, Margaret M. Murnane, and Giulia F. Mancini. Subwavelength coherent imaging of periodic samples using a 13.5nm tabletop high-harmonic light source. *Nature Photonics*, 11(4):259–263, 2017.

[8] Elisabeth R. Shanblatt, Christina L. Porter, Dennis F. Gardner, Giulia F. Mancini, Robert M. Jr. Karl, Michael D. Tanksalvala, Charles S. Bevis, Victor H. Vartanian, Henry C. Kapteyn, Daniel E. Adams, and Margaret M. Murnane. Quantitative chemically specific coherent diffractive imaging of reactions at buried interfaces with few nanometer precision. *Nano Letters*, 16(9):5444–5450, 2016.

[9] Wilhelm Eschen, Lars Loetgering, Vittoria Schuster, Robert Klas, Alexander Kirsche, Lutz Berthold, Michael Steinert, Thomas Pertsch, Herbert Gross, Michael Krause, Jens Limpert, and Jan Rothhardt. Material-specific high-resolution table-top extreme ultraviolet microscopy. *Light: Science and Applications*, 11(1):117, 2022.

[10] Chang Liu, Wilhelm Eschen, Lars Loetgering, Daniel S Penagos Molina, Robert Klas, Alexander Iliou, Michael Steinert, Sebastian Herkersdorf, Alexander Kirsche, and Thomas Visualizing the ultra-structure of microorganisms using table-top extreme ultraviolet imaging. 4(1):6, 2023.

[11] Darren J. Batey, Daniel Claus, and John M. Rodenburg. Information multiplexing in ptychography. *Ultramicroscopy*, 138:13–21, 2014.

[12] Pierre Thibault and Andreas Menzel. Reconstructing state mixtures from diffraction measurements. *Nature*, 494(7435):68–71, 2013.

[13] Bosheng Zhang, Dennis F. Gardner, Matthew H. Seaberg, Elisabeth R. Shanblatt, Christina L. Porter, Robert Karl, Christopher A. Mancuso, Henry C. Kapteyn, Margaret M. Murnane, and Daniel E. Adams. Ptychographic hyperspectral spectromicroscopy with an extreme ultraviolet high harmonic comb. *Optics Express*, 24(16):18745–18754, 2016.

[14] Tao Sun, Zhang Jiang, Joseph Strzalka, Leonidas Ocola, and Jin Wang. Three-dimensional coherent x-ray surface scattering imaging near total external reflection. *Nature Photonics*, 6(9):586–590, 2012.

[15] Matthew D. Seaberg, Bosheng Zhang, Dennis F. Gardner, Elisabeth R. Shanblatt, Margaret M. Murnane, Henry C. Kapteyn, and Daniel E. Adams. Tabletop nanometer extreme ultraviolet imaging in an extended reflection mode using coherent fresnel ptychography. *Optica*, 1(1):39–44, 2014.

[16] Robert M. Karl, Giulia F. Mancini, Joshua L. Knobloch, Travis D. Frazer, Jorge N. Hernandez-Charpak, Begoña Abad, Dennis F. Gardner, Elisabeth R. Shanblatt, Michael Tanksalvala, Christina L. Porter, Charles S. Bevis, Daniel E. Adams, Henry C. Kapteyn, and Margaret M. Murnane. Full-field imaging of thermal and acoustic dynamics in an individual nanostructure using tabletop high harmonic beams. 4(10):eaau4295, 2018.

[17] Michael Tanksalvala, Christina L. Porter, Yuka Esashi, Bin Wang, Nicholas W. Jenkins, Zhe Zhang, Galen P. Miley, Joshua L. Knobloch, Brendan McBennett, Naoto Horiguchi, Sadegh Yazdi, Jihan Zhou, Matthew N. Jacobs, Charles S. Bevis, Robert M. Karl, Peter Johnsen, David Ren, Laura Waller, Daniel E. Adams, Seth L. Cousin, Chen-Ting Liao, Jianwei Miao, Michael Gerrity, Henry C. Kapteyn, and Margaret M. Murnane. Nondestructive, high-resolution, chemically specific 3d nanostructure characterization using phase-sensitive euv imaging reflectometry. 7(5):eabd9667, 2021.

[18] Yifeng Shao, Sven Weerdenburg, Jacob Seifert, H Paul Urbach, Allard P Mosk, Wim Wavelength-multiplexed multi-mode euv reflection ptychography based on automatic differentiation. 13(1):196, 2024.

[19] Christina L. Porter, Michael Tanksalvala, Michael Gerrity, Galen Miley, Xiaoshi Zhang, Charles Bevis, Elisabeth Shanblatt, Robert Karl, Margaret M. Murnane, Daniel E. Adams, and Henry C. Kapteyn. General-purpose, wide field-of-view reflection imaging with a tabletop 13&#x2009;&#x2009;nm light source. *Optica*, 4(12):1552–1557, Dec 2017.

[20] Nathan J. Brooks, Bin Wang, Iona Binnie, Michael Tanksalvala, Yuka Esashi, Joshua L. Knobloch, Quynh L. D. Nguyen, Brendan McBennett, Nicholas W. Jenkins, Guan Gui, Zhe Zhang, Henry C. Kapteyn, Margaret M. Murnane, and Charles S. Bevis. Temporal and spectral multiplexing for euv multibeam ptychography with a high harmonic light source. *Opt. Express*, 30(17):30331–30346, Aug 2022.

[21] Pavel Sidorenko and Oren Cohen. Single-shot ptychography. *Optica*, 3(1):9–14, 2016.

[22] Hannah C. Strauch, Fengling Zhang, Stefan Mathias, Thorsten Hohage, Stefan Witte, and G. S. Matthijs Jansen. Fast spectroscopic imaging using extreme ultraviolet interferometry. *Optics Express*, 32(16):28644–28654, 2024.

[23] Andrew M Maiden, Martin J Humphry, and John M Ptychographic transmission microscopy in three dimensions using a multi-slice approach. 29(8):1606–1614, 2012.

[24] Dennis F. Gardner, Bosheng Zhang, Matthew D. Seaberg, Leigh S. Martin, Daniel E. Adams, Farhad Salmassi, Eric Gullikson, Henry Kapteyn, and Margaret Murnane. High numerical aperture reflection mode coherent diffraction microscopy using off-axis apertured illumination. *Optics Express*, 20(17):19050–19059, 2012.

[25] Pengming Song, Ruihai Wang, Jiakai Zhu, Tianbo Wang, Zichao Bian, Zibang Zhang, Kazunori Hoshino, Michael Murphy, Shaowei Jiang, Chengfei Guo, and Guoan Zheng. Super-resolved multispectral lensless microscopy via angle-tilted, wavelength-multiplexed ptychographic modulation. *Optics Letters*, 45(13):3486–3489, 2020.

[26] Stefan Witte, Vasco T. Tenner, Daniel W. E. Noom, and Kjeld S. E. Eikema. Lensless diffractive imaging with ultra-broadband tabletop sources: from infrared to extreme-ultraviolet wavelengths. *Light: Science and Applications*, 3(3):e163–e163, 2014.

[27] Minh Pham, Arjun Rana, Jianwei Miao, and Stanley Semi-implicit relaxed douglas-rachford algorithm (sdr) for ptychography.

27(22):31246–31260, 2019.

[28] Charles Bevis, Robert Karl, Jonathan Reichanadter, Dennis F. Gardner, Christina Porter, Elisabeth Shanblatt, Michael Tanksalvala, Giulia F. Mancini, Henry Kapteyn, Margaret Murnane, and Daniel Adams. Multiple beam ptychography for large field-of-view, high throughput, quantitative phase contrast imaging. *Ultramicroscopy*, 184:164–171, 2018.

[29] Tsumoru Shintake. *Phys. Rev. E*, 78:041906, Oct 2008.

[30] Chi-Feng Huang, Wei-Hau Chang, Ting-Kuo Lee, Yasumasa Joti, Yoshinori Nishino, Takashi Kimura, Akihiro Suzuki, Yoshitaka Bessho, Tsung-Tse Lee, and Mei-Chun Xfel coherent diffraction imaging for weakly scattering particles using heterodyne interference. 10(5), 2020.

[31] Hyeon-ho Son and Kyunghwan Oh. Light propagation analysis using a translated plane angular spectrum method with the oblique plane wave incidence. *Journal of the Optical Society of America A*, 32(5):949–954, 2015.